# Electronic structure and bonding in crystalline peroxides

Markus Königstein, Alexei A. Sokol, and C. Richard A. Catlow
*Davy Faraday Research Laboratory, The Royal Institution of Great Britain, 21 Albemarle Street, London W1X 4BS, United Kingdom*
(Received 4 March 1998; revised manuscript received 18 March 1999)

Hartree-Fock and density-functional PW91 theories as realized in the CRYSTAL95 code have been applied to investigate the structural and electronic properties of Ba, Sr, and Ca peroxide materials with the calcium carbide crystal structure, results for which are compared with those for the corresponding oxides. Special attention is paid to the stabilization of the peroxide molecular ion $O_2^{2-}$ in the ionic environment provided by the lattice, and to chemical bonding effects. In order to describe the covalent bonding within the $O_2^{2-}$ ion and the polarization of the $O^-$ ion in the crystal electrostatic field, it is essential to include an account of the effects of electron correlation. The PW91 density functional has allowed us to reproduce the crystallographic parameters within a 3% error. The chemical bonding within the peroxide molecular ion has a complex nature with a balance between the weak covalent bond of $\sigma_z$ type and the strong electrostatic repulsion of the *closed-shell* electron groups occupying O $2s$ and O $2p_x$ and $2p_y$ states. Compression of the peroxide ion in the ionic crystals gives rise to an excessive overlap of the O $2s$ closed shells of the two $O^-$ ions of a peroxide molecular ion $O_2^{2-}$, which in turn determines *the antibonding character of the interaction and chemical bonding in the* $O_2^{2-}$ *molecular ion*. [S0163-1829(99)09527-2]

## I. INTRODUCTION

For many years, the peroxide ion $O_2^{2-}$ has been the focus of interest in solid-state physics, since the species is present in most oxide materials as an important defect center with interesting physical and chemical properties.[1,2] As shown theoretically,[3] this ion is metastable as an isolated molecule, which implies that it must be stabilized by its environment. Such stabilization can result from covalent bonding, as in, for example, hydrogen peroxide,[4] or from electrostatic interactions in ionic crystals.[5,6] Indeed, the anionic sublattice of $O_2^{2-}$ ions is stabilized in $BaO_2$, $SrO_2$, and related crystalline compounds, as shown in a recent theoretical study.[7] Here, we concentrate on the electronic and structural properties of this latter class of materials. Our work reveals surprising features of the bonding in these materials. Our study is also relevant to the properties of peroxy anions in solids and indeed to polyanionic compounds in general.

In spite of the multitude of crystal structures and chemical bonding effects in which the peroxide molecular ion is involved, certain fundamental properties show little variation. In particular, the peroxide bond lengths of simple crystalline ionic peroxides and of crystalline hydrogen peroxide normally lie in the range 1.45–1.54 Å (Refs. 8–12) and their stretching vibrations are between 730 and 930 $cm^{-1}$ (Ref. 13). Experimental data available for alkaline-earth-metal peroxides fall within these ranges; other physical properties, e.g., electronic structure and elastic constants, presently remain undetermined. Theoretical investigations of these materials also pose problems. Localization of electron density over a small region in the lattice occupied by $O_2^{2-}$ would be expected to lead to an increased importance of electron correlation, which cannot be investigated by traditional one-electron or Hartree-Fock (HF) theories. The density-functional theory (DFT) using nonlocal density approximations presents probably the best approach as it provides a relatively cheap and sufficiently accurate treatment of correlation, compared with more traditional post-HF methods of quantum chemistry.

In the past ten years, *ab initio* quantum-mechanical techniques have been increasingly used for the investigation of the structural and electronic properties of crystalline compounds. The alkaline-earth-metal oxides were amongst the first compounds studied with such methods,[14,15] as they crystallize in the highly symmetric wurtzite or rocksalt structures whose small unit cells facilitate the use of computational methods. Various properties, including the equilibrium structures and cohesive energies, electronic and lattice dynamical properties, elastic constants and phase transitions have been successfully modeled.[14,16,17] In contrast, there are no quantum-mechanical studies of the crystalline alkaline-earth-metal peroxides, although barium peroxide, for example, is a chemically important compound and crystallizes also in a simple, symmetric structure.

These compounds possess a tetragonally distorted rock salt structure, usually referred to as the calcium carbide structure—space group I4/mmm. The metal ions occupy the regular cation positions and the peroxide dumbbells ($O_2^{2-}$) are centered on the anion sites, while their alignment is along one of the unit cell axes ($c$ axis) leading to the observed tetragonal structure, as shown in Fig. 1. Crystallographic studies of barium[9,18,19] and strontium peroxide[9,20] are based on single-crystal x-ray diffraction, while that of calcium peroxide is based on powder diffraction data[21,22] of poorly crystalline samples, which are not pure calcium peroxide but also contain water and/or hydrogen peroxide. They show additional weak reflections that cannot be attributed to the calcium carbide structure,[9,21] and the crystal structure reported for calcium peroxide cannot be considered as reliable.

The previous relevant quantum-mechanical calculations on peroxides comprise various studies on peroxide molecules including hydrogen peroxide and different inorganic and organic peroxide defect centers in the bulk and on the surfaces

 

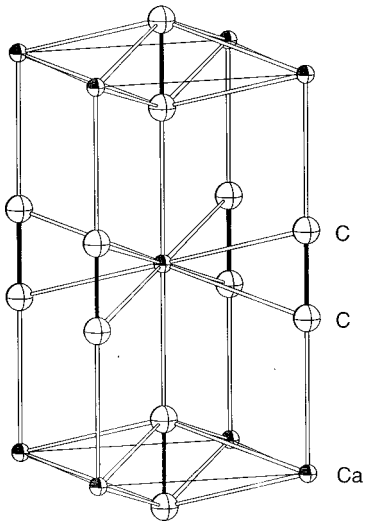


FIG. 1. The calcium carbide structure.

of crystalline and amorphous materials.[23–31] The investigation in this paper focuses on the structural and electronic properties of the crystalline calcium carbide-structured peroxides of barium, strontium, and calcium making detailed comparison with the corresponding oxides. We place a special emphasis on the properties of the peroxide bond and compare results obtained for the three different peroxides. Furthermore, we compare results for Hartree-Fock and density-functional theory-based methods.

Our paper is organized as follows: after a brief description of the methodological aspects in the next section, we discuss first the electronic properties of the peroxides at equilibrium, which are compared to those of the corresponding oxides: charge-density distribution associated with the peroxide ions plays a key rôle in understanding the unique properties of these materials. Next, the optimized structures are compared with the experimental data; we also investigate the behavior of the structure under pressure and compare the results with the available experimental data.

## II. METHODOLOGY

The quantum-mechanical, electronic calculations have been performed using a periodic self-consistent field approach as described in the monograph of Pisani, Dovesi, and Roetti[32] and realized in the CRYSTAL95 program package.[33] Both the method and the program have been widely used in recent years and a detailed review is unnecessary. We will only outline, therefore, the major features of the approach and the technical details appropriate to its application in this study.

Presently, the program allows calculations with HF and DFT methods (in a recent implementation described by Causà and Zupan[34]), based on expansion of crystal orbitals in linear combinations of Gaussian-type atomic orbitals (LCAO). A number of local and non- (or semi-) local density functionals are available in the program, but we have chosen the Perdew-Wang gradient-corrected exchange and correlation functionals[35,36] (PW91) for the following methodological and practical reasons:

TABLE I. Valence basis set (exponents and contraction coefficients of the Gaussian functions) adopted for Ba.[a] The basis set has been used along with the Hay-Wadt small-core pseudopotential.[b]

| Shell type | Exponents [Bohr$^{-2}$] | Coefficients $s$ | Coefficients $p,d$ |
|---|---|---|---|
| $5sp$ | 2.5964 | 0.1355 | −0.0141 |
| | 1.3877 | −0.7698 | −0.19759 |
| | 0.5565 | 0.8298 | 0.58272 |
| $6sp$ | 0.274 | 1.0 | 1.0 |
| $7sp$ | 0.153 | 1.0 | 1.0 |
| $3d$ | 1.7718 | | −0.0249 |
| | 0.4465 | | 0.700 |
| | 0.136 | | 0.405 |

[a]Reference 40.
[b]Reference 39.

(i) The derivation of the PW91 functional used fully *ab initio* techniques with particular care being taken in reproducing the asymptotic behavior of the exchange-correlation hole. Furthermore, other functionals include semiempirical parameters fitted using reference sets of small molecules and are not, therefore, the most appropriate for these highly ionic crystals.

(ii) Application of the PW91 functionals in solid-state calculations has proved their accuracy and reliability for very different systems: metallic,[36] covalent,[37] ionic,[37] and hydrogen bonded.[38] In alkaline-earth-metal peroxides, we naturally expect to find a dramatic change in the chemical bonding and charge-density behavior on the atomic scale as we pass from a homopolar environment within the peroxide anions to a heteropolar one between cationic and anionic sublattices.

All-electron basis sets have been employed in this paper for oxygen and calcium, while strontium and barium were represented by Hay-Wadt small-core pseudopotentials[39] and valence-electron basis sets. The choice of pseudopotentials for heavier atoms is, as usual, dictated by the need to include relativistic effects for more energetic core electrons, on the one hand, and by a significant decrease in the computational cost resulting from the reduced number of electrons treated explicitly. For Ca, Sr, and Ba, we have used basis sets derived in Refs. 16, 17, and 40 (previously unpublished parameters of the Ba basis set are listed in Table I), while the basis set for O has been taken from Ref. 41 using the exponents 0.500, 0.191, and 1.000 Bohr$^{-2}$ for the $3sp$, $4sp$, and $3d$ shells, respectively.

We note that the presence of the optimized $3d$ shell in the oxygen basis set is crucial for the description of the peroxides. For example, the presence of the $3d$ orbital lowers the total energy of $BaO_2$ in our Hartree-Fock calculations by more than 0.013 hartrees, while for BaO the difference for calculations with and without $d$ orbitals is only $10^{-4}$ hartrees. The importance of the oxygen $3d$ orbitals for the description of the bonding within the peroxide bond will be shown later by an analysis of the electronic density of states (DOS). On the other hand, we found that the presence of the $3d$ shell in the oxygen basis set has little influence on the optimized geometries, except for a shortening of the peroxide bond length by approximately 0.05 Å. For a more direct comparison of results, we used the same oxygen basis set for

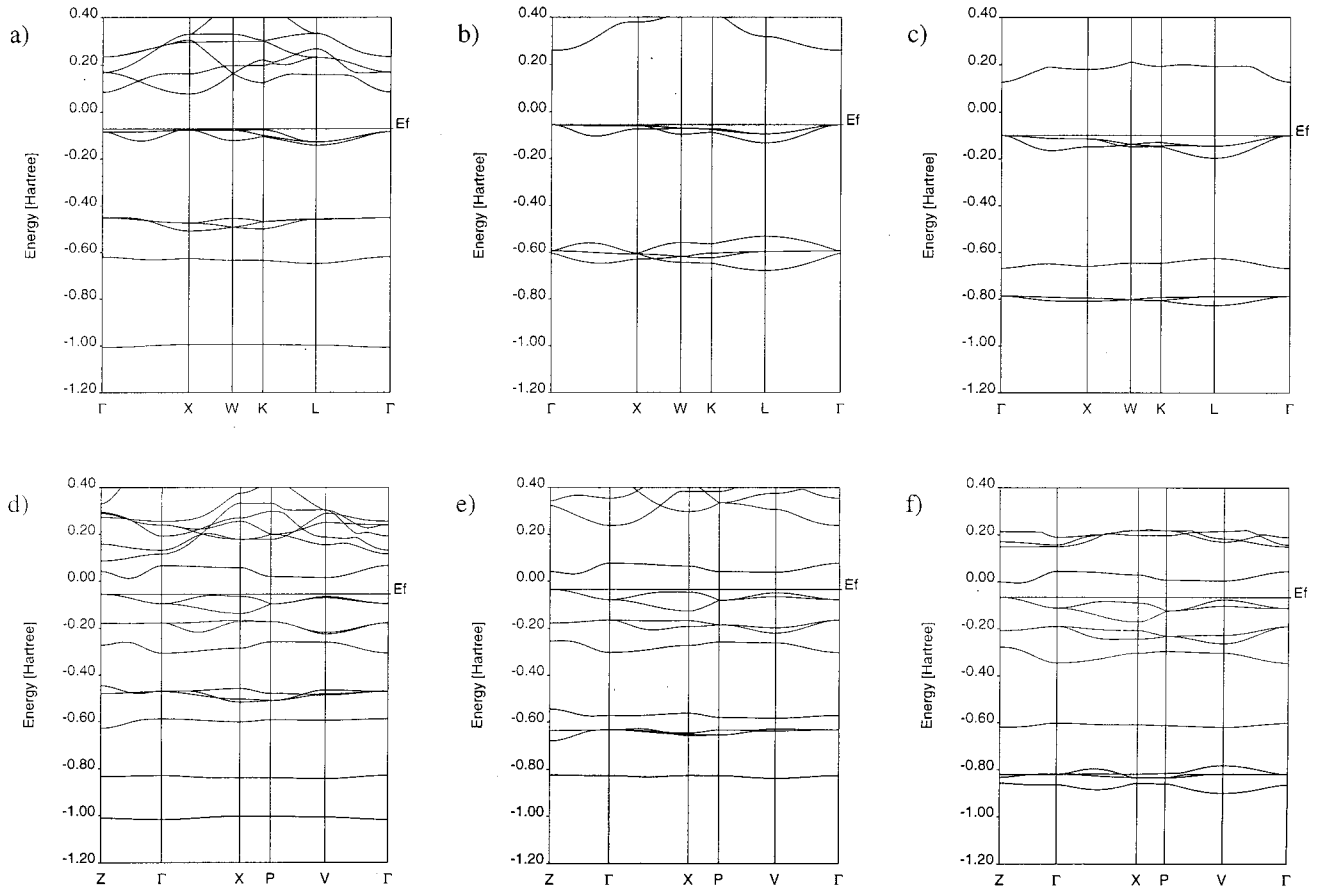


FIG. 2. Band structures of (a) BaO, (b) SrO, (c) CaO, (d) $BaO_2$, (e) $SrO_2$, and (f) $CaO_2$ (DFT calculations). *Ef* stands for the Fermi energy. The bands have been calculated in the directions of the first Brillouin zone as specified by the following special points: Oxides of the $Fm\bar{3}m$ space group $\Gamma(0,0,0)$; $X(1/2,0,1/2)$; $W(1/2,1/4,3/4)$; $K(3/8,3/8,3/4)$; $L(1/2,1/2,1/2)$. Peroxides of the I4/mmm space group $\Gamma(0,0,0)$; $Z(1/2,1/2,-1/2)$; $X(0,0,1/2)$; $P(1/4,1/4,1/4)$; $V(0,1/2,0)$.

both oxide and peroxide ions in both Hartree-Fock and DFT calculations.

Both basis sets and pseudopotentials were derived on the basis of HF calculations, which may lead to some uncertainty regarding the quality of the DFT results. However, the properties considered in this paper do not explicitly involve core electrons; thus, we expect that only small corrections of a uniform character should follow the introduction of the DFT pseudopotential. Next, the extended character of triple-split valence basis set used provides a large degree of variational freedom so that a reoptimization of the basis set parameters should not lead to significant changes in the properties predicted. We also note that the spin-orbital interaction can have some importance in the electronic spectra of the Ba compounds relating to charge transfer to the Ba; such processes are not of particular interest here.

## III. ELECTRONIC PROPERTIES AT EQUILIBRIUM

Electronic band structure and density of states often provide sufficient data for a thorough characterization of the electronic properties of materials; however, this spectroscopic information does not describe the specific character of the chemical bonding in the system. A major focus of this study concerns the properties of the peroxide anion and its contribution to the properties of the material as a whole. Charge-density distributions and population analyses are therefore employed as a complementary tool for the characterization of the electronic structure. In the discussion that follows all results on the electronic properties have been obtained for the optimized crystal structures.

### A. Band structure and density of states

The present calculations of the electronic structure show that the electronic states associated with the oxide and peroxide ions provide a dominant contribution to the valence bands in all materials considered, irrespective of the method applied. The main difference between the different oxides and peroxides is related to the cation semicore states (the highest occupied shells on the cations) whose position changes with respect to the other bands, the Ca-associated bands being the lowest and the Ba bands the highest. Otherwise, the band structures within each group (of oxides and peroxides) are qualitatively similar,[9] and we mostly concentrate here on the Ba compounds.

The band structures of BaO and $BaO_2$, obtained from the DFT calculations, are presented in Figs. 2(a) and 2(d) in the high-symmetry directions of the first Brillouin zone. The electronic bands are flat as expected for ionic compounds.

For BaO, the direct band gap at the $\Gamma$ point is 4.6 eV compared with the experimental value[42] of 4.29 eV while the indirect $\Gamma$-$X$ band gap is slightly smaller[43] at 4.4 eV. The corresponding band gap at the $\Gamma$ point for $BaO_2$ is 4.4 eV, but experimental data are unavailable for comparison. The close agreement of the calculated and experimental band gap for BaO at the $\Gamma$ point should be treated cautiously as the DFT one-electron spectra are known to underestimate the interband gap, in particular, owing to an incomplete account of the self-interaction; the relatively wide gap can probably be related to a limited size of the basis set used and the localized character of the basis functions.

If we consider the occupied bands in more detail, using information on the atomic orbital representation of the crystal orbitals at the $\Gamma$ point, we can see that the three bands at around $-0.46$ hartrees and the band at around $-1.01$ hartrees appear in both band structures and are mainly of Ba $5p$ and $5s$ character, respectively. The remaining occupied bands correspond to the O $2p$ and $2s$ atomic states. Hence, the corresponding atomic and crystalline states will be used below for designation of the electronic bands.

While in BaO, the topmost occupied O $2p$ bands are degenerate at the $\Gamma$ point—we find in $BaO_2$ the expected splitting of the O $2p$ atomic levels at the $\Gamma$ point into the peroxide bonding $\sigma_z$ ($-0.31$ hartrees), degenerate bonding $\pi_x$ and $\pi_y$ ($-0.18$ hartrees), degenerate antibonding $\pi_x^*$ and $\pi_y^*$ ($-0.10$ hartrees) and unoccupied antibonding $\sigma_z^*$ (0.07 hartrees) bands, the latter giving rise to the lowest conduction band. The O $2s$ level in $BaO_2$ is split similarly into the peroxide bonding $\sigma_s$ ($-0.83$ hartrees) and antibonding $\sigma_s^*$ ($-0.59$ hartrees) bands, while in BaO there is only one O $2s$ band at $-0.62$ hartrees at the $\Gamma$ point. Thus, the splitting of the oxygen $s$ and $p$ atomic levels into the corresponding bands at the $\Gamma$ point of the band structure of $BaO_2$ corresponds with the classical molecular orbital diagram of the peroxide molecular ion and its isoelectronic molecule $F_2$.

The DOS for BaO and $BaO_2$ (Figs. 3 and 4, respectively) confirm the assignment of the bands made above. However, the plots indicate that the barium and oxygen orbitals mix significantly. In particular, the Ba $5s$ states play an important role in the formation of the O $2s\sigma_s$ band, reducing the charge density along the ionic bonds. As a result, the O $2s$ atomic orbitals are not fully orthogonal to the O $2p$ crystal orbitals, and contribute to the $\sigma_z$ bonding orbital of the O $2p_z$ character in $BaO_2$, in turn, reducing the charge density within the peroxide ion. The upper occupied states in $BaO_2$ consist not only of the peroxide bonding $\pi_{x,y}$ and antibonding $\pi_{x,y}^*$ molecular orbitals, but also of contributions from Ba $d$ orbitals. Furthermore, the DOS of $BaO_2$ show the contribution of the O $3d$ orbitals in the peroxides in contrast to the oxides. In particular, the $d(z^2)$ atomic orbital contributes about 0.6% to the maximum DOS of the peroxide $\sigma_s$ crystal orbital. Furthermore, to a smaller extent the $d(z^2)$ atomic orbital contributes to the peroxide $\sigma_z$ and $\sigma_z^*$ orbitals, while the $d(xz)$ and $d(yz)$ atomic orbitals contribute a small amount to the peroxide $\pi_x$ and $\pi_y$ crystal orbitals. The maximum contribution of the O $3d$ orbital in BaO, which corresponds to a hybridization of the O $d(z^2)$ atomic orbitals with the Ba $p$ atomic orbitals, is smaller by a factor of approximately 100 than in $BaO_2$. This behavior for BaO should be expected as

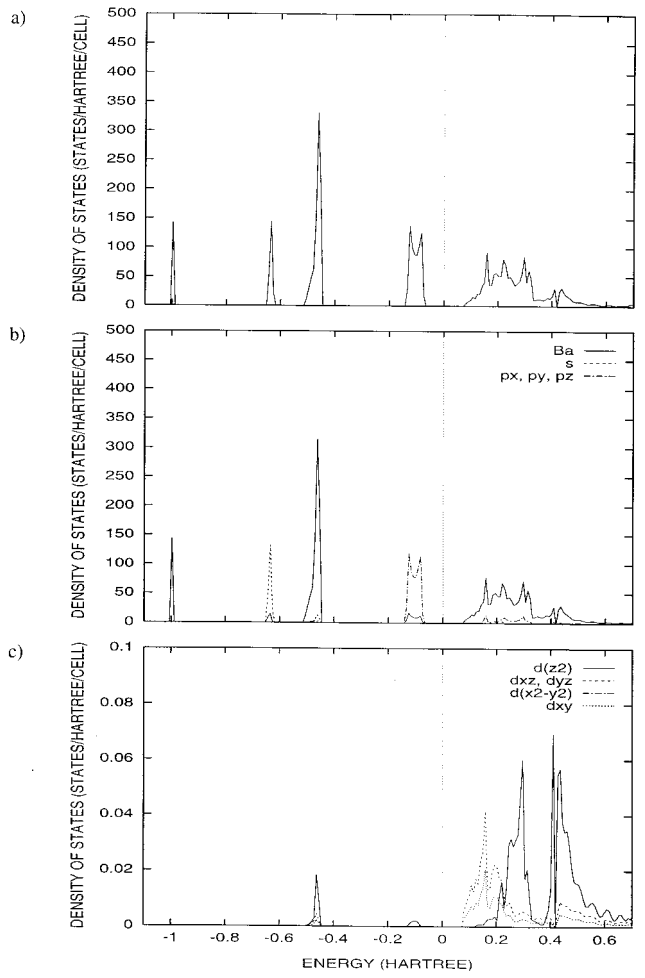


FIG. 3. DOS of BaO (DFT calculations). (a) Total DOS; projected DOS on: (b) the barium (Ba) and the oxygen $s$ ($s$), $p_x$ ($px$), $p_y$ ($py$), and $p_z$ ($pz$) atomic orbitals; (c) the oxygen $d$ atomic orbitals.

the system is highly ionic, the ions are situated at lattice sites of cubic symmetry (octahedral coordination), where the strongest dipolar term of the polarizing crystal field is zero, and the valence electrons on Ba and O are only of $s$ and $p$ character. A different situation occurs in $BaO_2$, where the oxygen ions are at the sites of a nonzero electrostatic field, which gives rise to strong electronic polarization effects. However, the absolute value of the $d$-functions' contribution varies with the basis set. Indeed, due to an overlap between Ba and O basis functions, a fraction of the electronic polarization on the $O^-$ ion is described by a charge transfer from the $O^-$ back to the $Ba^{2+}$ ions.

Looking at the formation of the electronic bands from a different angle, we conclude that the complex mechanism of the hybridization of O atomic states of different symmetry, triggered by the admixing of the Ba $5s$ states, is responsible for the polarization of the electronic density on the $O^-$ ions in $BaO_2$. Each of these ions is situated in the electric field directed along the $c$ axis (arising from the neighboring cation and O ion). The polarization of the $O^-$ ions by the lattice field substantially destabilizes the $\sigma_z$ states owing to the antibonding character of the O $2s$ contribution. Thus, the charge density on each $O^-$ associated with the O $2s\sigma_s$, $\sigma_s^*$

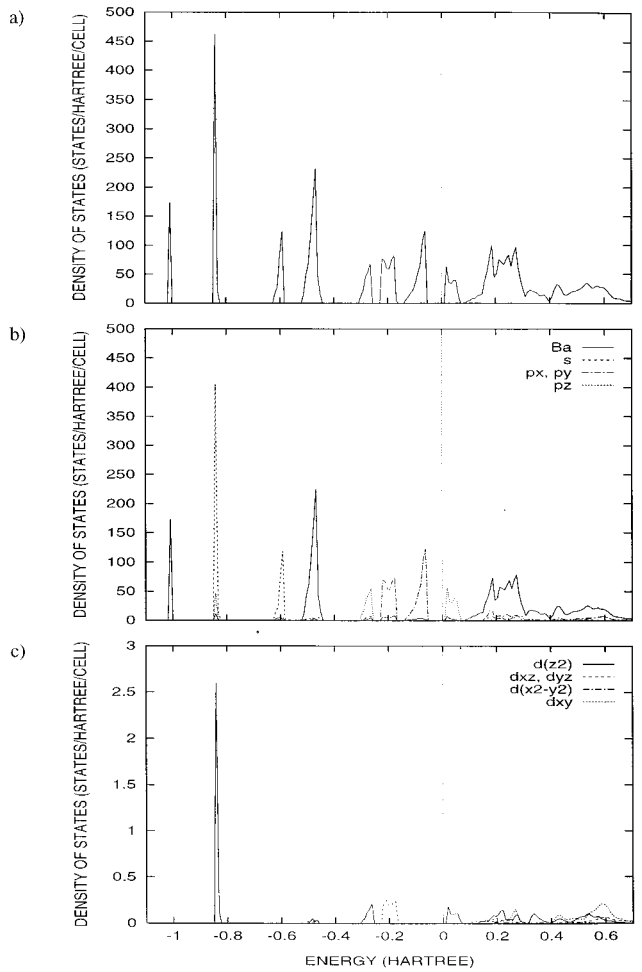


FIG. 4. DOS of $BaO_2$ (DFT calculations). (a) Total DOS; projected DOS on: (b) the barium (Ba) and the oxygen $s$ $(s)$, $p_x$ $(px)$, $p_y$ $(py)$, and $p_z$ $(pz)$ atomic orbitals; (c) the oxygen $d$ atomic orbitals.

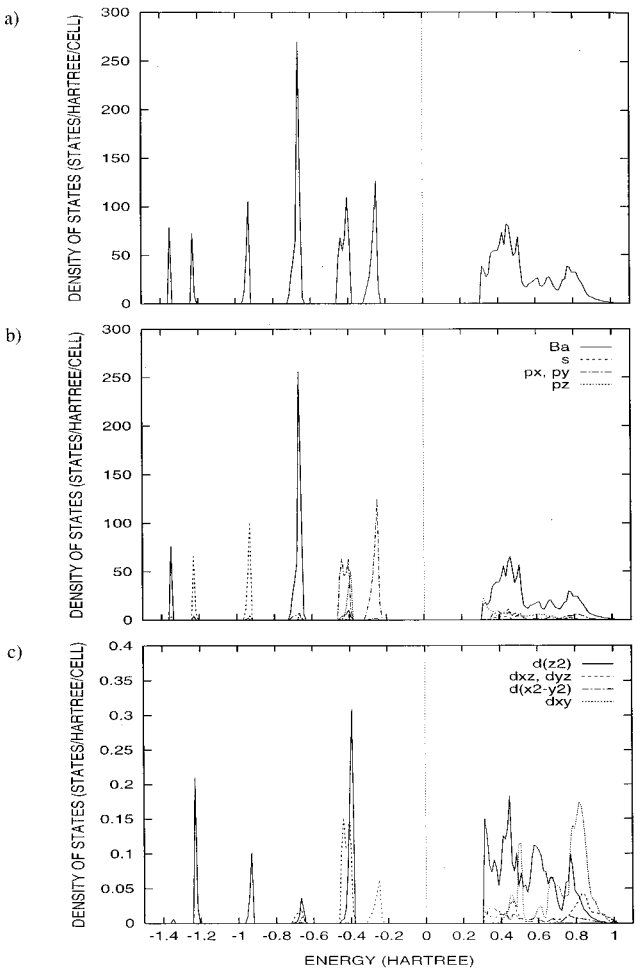


FIG. 5. DOS of $BaO_2$ (HF calculations). (a) Total DOS; projected DOS on (b) the barium (Ba) and the oxygen $s$ $(s)$, $p_x$ $(px)$, $p_y$ $(py)$, and $p_z$ $(pz)$ atomic orbitals; (c) the oxygen $d$ atomic orbitals.

bands is shifted inwards in the peroxide ion while the charge density associated with the O $2p\sigma_z$ band is expelled from the peroxide bonding region towards the nearest cations. A similar mechanism operates in all three peroxides. The major difference is mainly due to the fact that the metal $p$ bands in Sr and Ca peroxide appear between bonding and antibonding O $2s$ bands: the Sr $4p$ band at $-0.63$ hartrees is in close proximity to O $2s$ antibonding states, whereas the Ca $3p$ states at $-0.82$ hartrees nearly overlap with the O $2s\sigma_s$ band (Fig. 2).

Let us now compare the DOS of $BaO_2$ calculated using the DFT (Fig. 4) and the HF method (Fig. 5). Apart from the band gap in the HF DOS, which is, as expected, much larger than the DFT band gap, and the fact that the peaks in the HF valence band occur at energies different from those in the DFT calculations, we find two striking differences. First, we observe in the HF DOS that the order of the $\sigma_z$ and $\pi_{x,y}$ bands is reversed compared to the DFT calculations: the maximum of the peak of the $\sigma_z$ band is higher in energy than the two maxima of the peaks of the $\pi_x$ and $\pi_y$ crystal bands [Fig. 5(b)]. Second, the bottom of the conduction band is predicted, in the HF calculations, to consist, to an equal extent, of contributions from the O $\sigma_z^*$ and Ba $6p$ states; in contrast, the DFT calculations predict it to be predominantly of O $\sigma_z^*$ orbital character. This difference is clearly due to the neglect of electron correlation in the Hartree-Fock method: correlation is particularly important for regions in the crystal with high-electron density, in general, and for the description of a covalent bonding, in particular. Since the electron density is considerably higher in $\sigma$ than in $\pi$ bonds, the energy levels corresponding to the $\sigma$ bonding are stabilized by correlation relative to those corresponding to $\pi$ bonding. The neglect of correlation leads consequently to a destabilization of the O $\sigma_z$ and $\sigma_z^*$ crystal orbitals in the HF calculations, which in turn leads to the reversed order of the $\sigma_z$ and $\pi_x$ and $\pi_y$ bands in the HF and DFT calculations as well as to the different nature of the bottom part of the conduction band. Although without a proper calculation of the optical transitions, our predictions have only preliminary character, we can conclude that in peroxides we should expect on-site excitations to play a predominant role in contrast to oxides where charge transfer is a competing process: in BaO the charge transfer should be predominant, while in SrO and CaO our calculations indicate a small but increasing contribution of on-site processes. Moreover, both oxides and peroxides have metal $d$ bands closely following the lower

conduction bands, which suggests that under pressure, due to the localized character of the *d* shells on metal cations, they can be of importance (see the discussion in the following section). We conclude that the inclusion of electron correlation in *ab initio* quantum-mechanical calculations is crucial for peroxides, or alternatively, the Hartree-Fock method is unsuitable for a correct description of the peroxide bond.

### B. Character of the chemical bonding

As mentioned, the full information contained in the wave function can be represented in different ways: the density of states and the charge density being the simplest. Whereas the former has provided us with the first insight into the spectroscopic and electronic properties, the latter will be used here for a more thorough characterization of the bonding effects in the peroxide materials. Charge transfer from cations to anions is traditionally associated with the formation of ionic systems whereas the electron density concentration in interionic regions is an indication of covalent effects. We have applied two methods currently in a wide use to analyze these effects: the Mulliken population analysis and Bader's atoms in molecules (AIM) theory.[44,45] To facilitate the following discussion, we briefly recall next the basic points of these methods.

The Mulliken analysis is based on the LCAO approximation of the molecular-orbital theory. The bond population is defined by the appropriate nondiagonal elements of the density matrix in the AO representation scaled by the corresponding overlap integrals and summed over AOs centered on a given pair of atoms. Although the absolute values are heavily dependent on the quality of the basis set employed (see a detailed discussion for example in Ref. 46), this analysis is successfully used wherever we are only concerned with relative changes in ion and bond population.

The AIM method uses solely the charge density $\rho$ for an analysis and thus its results only depend on the quality of a reproduction of $\rho$. At the heart of the AIM approach is the definition of an atom as an open system separated from other atoms by an interface: the surface of zero flux in the gradient vector field of $\rho$. The $\rho$ distribution along the lines connecting atoms defines in this theory the character of the bonding. Use of critical points $\mathbf{r}_c$ in the $\rho$ distribution, in which $\nabla\rho = 0$, allows the quantification of the corresponding information: of particular importance are the local maxima, situated nearly always at the nuclei (except for some metallic systems), and the points where the interatomic surface is crossed by the bond paths. The latter, referred to as the bonding $\mathbf{r}_c$ below, are the points of a minimum of $\rho$ on the bond path and the points of a maximum for perpendicular directions, which is reflected by the signature of the eigenvalues of the Hessian of $\rho$: one value is positive and two values are negative.

The sum of these eigenvalues, the Laplacian of $\rho$, is directly related to the character of the interatomic interaction by the local virial theorem[47]

$$\frac{\hbar^2}{4m}\Delta\rho(\mathbf{r}) = 2G(\mathbf{r}) + V(\mathbf{r}), \tag{1}$$

where $G$ and $V$ are electron kinetic and potential energy densities. Since $G$ is positive and $V$ is negative (for bounded electrons), one can conclude that the larger the electron kinetic-energy contribution, the more positive is the Laplacian of $\rho$ and, on contrary, the larger the potential-energy contribution, the lower is the value of $\Delta\rho$. In early publications,[45] Bader actually proposed to distinguish between two kinds of chemical bonding: the shared interaction as in the covalent bond characterized by a negative $\Delta\rho$ and the close-shell interaction occurring in ionic, molecular, and other compounds and characterized by a positive $\Delta\rho$. In particular, the shared interactions are accompanied by a concentration of the charge density on the bond, the electron distribution being shifted towards the bonding critical point both from ions along the bond path and from the directions perpendicular to the bond path. Thus, a strong chemical bond is expected in this theory to be characterized by negative values of $\Delta\rho$ and by large values of $\rho$ itself at the bonding $\mathbf{r}_c$.

Summarizing our intuitive ideas on the chemical bonding in peroxides, we should expect:

(i) a very small and maybe negative overlap population between metal ions and oxygen, which reflects an ionic character of the bonding; i.e., the charge density at a critical bonding point should also be small, while its Laplacian should be small and positive;

(ii) a large positive overlap population between the two oxygen ions forming a peroxy species, as should be the case for a covalent bond; accordingly, large values of the charge density should be accompanied by negative values of its Laplacian.

However, a Mulliken analysis on the basis of our DFT calculations confirms only the first assumption: the overlap (bond) population being $-0.003$, $-0.015$, and $+0.004$ $e$ for $BaO_2$, $SrO_2$, and $CaO_2$, respectively. The overlap population between the two oxygen ions of the peroxy species proves to be rather large and negative of $-0.126$, $-0.144$, and $-0.141$ $e$ for $BaO_2$, $SrO_2$, and $CaO_2$, respectively, i.e., an antibonding effect of the electrostatic repulsion seems to prevail over the covalent $\sigma_z$ bond between the $O^-$ ions. The largest contributions to the negative overlap are due to the overlap between:

(i) O $2s$ AOs, centered on the two oxygen ions, which suggests an overlap of the $2s$ closed-shell orbitals of the oxygen ions;

(ii) O $2p_x$ and O $2p_y$ AOs, centered on the two oxygen ions; this is an overlap involving both bonding and antibonding crystal orbitals of $\pi$ character; and, finally,

(iii) O $2s$ and O $2p_z$ AOs, centered on the two oxygen ions within the peroxy ion, which confirms an antibonding character of the admixture of the O $2s$ states to the $\sigma_z$ valence band.

In all three cases we observe an overlap between closed-shell orbitals centered on the two O ions of the peroxide molecular ion.

The trends outlined above are clearly corroborated by the behavior of the charge density at the critical bonding points. All corresponding data are collected in Table II. The positions of critical points, charge densities, and relevant values of the density Laplacian have been obtained manually on the basis of the calculated charge density. As a result the numerical values of the density Laplacian may lack some precision, but are sufficient for the purposes of the following analysis.

TABLE II. Values of the total charge densities $\rho$ and the density Laplacian at the minima of the total charge density: (a) within the O—O bond, (b) within the $M$—O bond, and (c) between two adjacent $O^-$ ions of neighboring peroxide molecular ions in the (110) plane.

| Compound | Total charge density (a.u.) | | | Laplacian (a.u.) | | |
|---|---|---|---|---|---|---|
| | (a) | (b) | (c) | (a) | (b) | (c) |
| $BaO_2$ | 0.2341 | 0.0234 | 0.0075 | 0.2023 | 0.1128 | 0.0220 |
| $SrO_2$ | 0.2339 | 0.0215 | 0.0107 | 0.2045 | 0.1216 | 0.0285 |
| $CaO_2$ | 0.2335 | 0.0167 | 0.0125 | 0.2159 | 0.1002 | 0.0386 |
| $O_2^{2-}$ | 0.1718 | | | 0.2610 | | |
| $H_2O_2$ | 0.2658 | | | 0.0737 | | |

Both in $BaO_2$ and BaO, the largest electron concentration is, as expected, found on the O ions. The charge density obtained by integration of the O $2s$ band is continuous in the interoxygen region, and prevails over the O $2p\sigma_z$ contribution. The charge density associated with $\pi$ and $\pi^*$ peroxide states is practically axially symmetrical around the $O_2^{2-}$ bond. The contribution to the valence density from Ba is also appreciable in the Ba region, which confirms the rôle of Ba states in the formation of the valence band and in the chemical bonding in the peroxides.

On examining the charge density within the peroxide ion, we find it behaves quite differently. Indeed, we observe a large concentration of the charge density in the bonding region and the corresponding value at the critical bonding point is practically the same of 0.234 a.u. in all peroxides (Table II). However, the density Laplacian is largely positive, which, again, points to an interaction of two closed-shell systems. The value of the Laplacian increases in the series of Ba, Sr, and Ca peroxides indicating an increased destabilization of the materials. However, both Mulliken and Bader approaches clearly demonstrate, that antibonding effects, or in other words, repulsive forces, prevail in the bonding character of the peroxide molecular ion. A comparison with the metastable, free molecular ion $O_2^{2-}$ shows that an ionic environment stabilizes the bond: the Laplacian decreases by approximately 0.05 a.u.; on the other hand, the charge density at the bonding critical point increases by ca. 0.07 to 0.234 a.u. The covalent type of the environment represented in our calculations of a free molecular $H_2O_2$ species[48] clearly provides a much higher stabilizing effect, which can be seen both from the molecular-orbital levels and from the relevant values in Table II. The value of $\rho$ at the peroxide bonding $\mathbf{r}_c$ increases to 0.266 a.u. while the density Laplacian decreases to 0.074 a.u.; the value is still positive but more than three times lower than in the free peroxide molecular ion. Furthermore, the Mulliken overlap (bond) population is $+0.072\ e$ for $H_2O_2$, indicating that we have a classical covalent bond in the peroxy species in $H_2O_2$.

In both ionic and covalent cases, the stabilization of the peroxy species in $H_2O_2$ and the crystalline peroxides is accompanied by a decrease in the peroxide bond lengths: from 1.64 Å in the free $O_2^{2-}$ species to 1.53 Å in the Ba, Sr, and Ca peroxides or to 1.48 Å in the $H_2O_2$ molecule. However, the nature of the stabilization is quite different. In the solid ionic environment, the electrostatic interaction with the lattice decreases the peroxide bond length. The constituent ions are therefore under the *pressure* generated by the increased short-range exchange correlation due to the surrounding ions. In the $H_2O_2$, the interoxygen repulsion is rather decreased due to an incomplete electron transfer from the hydrogen atoms. Both examples of $H_2O_2$ and $F_2$ molecules ($\Delta\rho$ being 0.074 and 0.787 a.u., respectively), in fact, demonstrate that Bader's description of the shared interactions, as characterized by negative values of the density Laplacian, does not apply in general. The trend in the Laplacian as outlined above is rather of interest, and lower values are indicating an increase in the chemical bonding.

## IV. STRUCTURAL PROPERTIES

### A. Crystal structure optimization

The calcium carbide structure of the alkali-earth-metal peroxides is defined by three crystallographic parameters: the two lattice constants $a$ and $c$ of the tetragonal unit cell and the oxygen fractional coordinate $z(O)$ that is also related to the peroxide bond length $d_{O—O}$ by the following relationship:

$$d_{O—O}=[1-2z(O)]c. \tag{2}$$

We selected six values of the unit cell volume ($V=a^2c$) of each peroxide and then calculated the total HF and DFT ground-state energy $E(V)$ by allowing each of the three crystallographic parameters fully to relax. The $E(V)$ data have been fitted here using the Vinet equation of state[49,50]

$$E(V)=-9V_0B_0e^{\gamma(1-\beta)}\left(\frac{1}{\gamma^2}-\frac{1}{\gamma}+\frac{\beta}{\gamma}\right)+\text{const.} \tag{3}$$

with

$$\gamma=\frac{3}{2}(B_0-1)\quad\text{and}\quad\beta=\left(\frac{V}{V_0}\right)^{1/3}, \tag{4}$$

from which we have obtained $V_0$ (the unit cell volume at equilibrium), $B_0$ (the zero pressure bulk modulus) and $B'$ (the pressure derivative of $B$ at $p=0$). For the equilibrium volume $V_0$ we again allowed each of the three crystallographic parameters to relax, and thus obtained the equilibrium values $a_0$, $c_0$, and $z_0(O)$.

The procedure is simpler for the rocksalt-structured oxides that are defined only by one crystallographic parameter, the lattice constant $a$. Hence, we were able to increase the number of points, where the function $E(V)$ has been calculated, to 10. The resulting oxide parameters, $a_0=V_0^{1/3}$, $B_0$, and $B'$ are reported in Table III along with the crystallographic parameters for the peroxides.

The agreement of the DFT crystallographic parameters with the experimental values is very good (with the exception of $CaO_2$, which we discuss later): the lattice constant $a_0$ for the oxides is within a 0.6% of experiment, while the maximum errors for $a_0$, $c_0$, and $z(O)$ in $BaO_2$ and $SrO_2$ are $+0.9\%$, $+1.4\%$ and $-0.5\%$, respectively. The slight overestimation of $a_0$ and $c_0$ for the peroxides corresponds with the results obtained in other calculations using the DFT in the generalized gradient approximation (including the PW91 functional): the method often overestimates covalent and semicovalent bond lengths.[51,52] In particular, the peroxide bond length is overestimated by 2.5% in $BaO_2$ and 3.2% in

TABLE III. Calculated (Hartree-Fock and DFT calculations) and experimental structural parameters for the peroxides and oxides of barium, strontium, and calcium: the equilibrium lattice parameter(s) $a_0$ (and $c_0$), unit cell volume $V_0$, oxygen fractional coordinate $z(O)$, peroxide bond length $d_{O—O}$, zero pressure bulk modulus $B_0$ and its pressure derivative $B'$. The experimental crystallographic data for $BaO_2$ and $SrO_2$ are from Ref. 9, and for $CaO_2$ from Ref. 21. The bulk modulus for $BaO_2$ is obtained from the $p$-$V$ data reported in Ref. 9 ($p < 5$ GPa) by fitting them using the Vinet equation of state; the experimental data are insufficiently accurate to fit a reasonable value of $B'$, which is therefore fixed at 4.00, which is justified by comparison with similar materials. Relative deviations from experiment, in percent, are given in parentheses.

| $MO_2$ | Hartree-Fock | | | DFT | | | Experiment | | |
|---|---|---|---|---|---|---|---|---|---|
| | $BaO_2$ | $SrO_2$ | $CaO_2$ | $BaO_2$ | $SrO_2$ | $CaO_2$ | $BaO_2$ | $SrO_2$ | $CaO_2$ |
| $a_0$ (Å) | 3.92 (+3.0) | 3.65 (+2.4) | 3.40 (−4.0) | 3.84 (+0.9) | 3.58 (+0.5) | 3.29 (−7.1) | 3.806 | 3.563 | (3.54) |
| $c_0$ (Å) | 7.00 (+2.4) | 6.69 (+1.1) | 6.56 (10.8) | 6.93 (+1.4) | 6.70 (+1.3) | 6.65 (12.3) | 6.837 | 6.616 | (5.92) |
| $V_0$ (Å$^3$) | 107.6 (+9) | 89.17 (+6) | 76.00 (+2) | 102.3 (+3) | 85.89 (+2) | 72.17 (−3) | 99.03 | 83.99 | (74.2) |
| $z(O)$ | 0.3964 (+1.4) | 0.3916 (+1.0) | 0.3895 | 0.3896 (−0.3) | 0.3858 (−0.5) | 0.3850 | 0.3908 | 0.3879 | (0.39) |
| $d_{O—O}$ (Å) | 1.45 (−2.9) | 1.45 (−2.2) | 1.45 | 1.53 (+2.5) | 1.53 (+3.2) | 1.53 | 1.493 | 1.483 | (1.30) |
| $B_0$ (GPa) | 74.5 | 84.9 | | 72.3 | 90.4 | 107.5 | 64.0 | | |
| $B'$ | 4.03 | 4.67 | | 5.91 | 4.38 | 3.86 | (4.00) | | |
| $M$(O) | BaO | SrO | CaO | BaO | SrO | CaO | BaO | SrO | CaO |
| $a_0$ (Å) | 5.62 (+1.5) | 5.19 (+0.6) | 4.85 (+0.8) | 5.55 (+0.2) | 5.13 (−0.6) | 4.80 (−0.2) | 5.539[a] | 5.160[a] | 4.811[a] |
| $B_0$ (GPa) | 83.4 (+1) | 114.7 (+19) | 127.0 (+9) | 81.5 (−1) | 117.9 (22) | 124.7 (+7) | 82.5[b] | 96.5[b] | 116.3[b] |
| $B'$ | 4.48 | 5.13 | 4.12 | 4.71 | 4.19 | 4.14 | 5.37[b] | 5.08[b] | 4.79[b] |

[a]Reference 54.

[b]These bulk moduli, linearly extrapolated to 0 K, and their derivatives are from Chang and Graham (Reference 55).

$SrO_2$, which also explains why the error in $c_0$ is higher than that in $a_0$, as the peroxide dumb bells are aligned along the $c$ axis of the unit cell. A relatively large elongation of the peroxide bond is, in fact, accommodated by a corresponding contraction of the ionic bonds so that the overall error in the reproduction of the $c$ lattice constant is not as large. The effect can be related to an underestimation of the polarizability of oxygen in the peroxide species, raising the question as to the quality of the basis set used.

HF crystallographic parameters are generally overestimated with respect to experiment (see also, e.g., Ref. 53) and the errors are clearly larger than in our DFT calculations: the lattice constants of the oxides are overestimated with a maximum error of 1.5% for BaO, while the maximum error for the crystallographic parameters of the peroxides $BaO_2$ and $SrO_2$ is 3.0%. On the other hand, we find that the peroxide bondlengths are underestimated by 2.9% in $BaO_2$ and 2.2% in $SrO_2$, which explains why the error in the lattice constant $c_0$ is somewhat smaller than in $a_0$.

Let us consider now the optimized structures for $CaO_2$. Both the HF and the DFT calculations largely disagree with the experimental data reported by Kotov[21] in 1941. The HF calculations, which in the case of $BaO_2$ and $SrO_2$ overestimated the structural parameters with a maximum error of 3%, predict that the $a_0$ lattice constant is *under*estimated by 4% with respect to experiment, while the $c_0$ lattice constant is *over*estmated by 10.8%. The DFT calculations, which reproduce for $BaO_2$ and $SrO_2$ structural parameters in good agreement with experiment, for $CaO_2$ give an even higher deviation: the $a_0$ value is underestimated by 7.1%, while $c_0$ is overestimated by 12.3%. The previous discussion of the band structure and charge-density distribution of the peroxides has already indicated that $CaO_2$ is less stable than $SrO_2$ and $BaO_2$. On the basis of the crystal-structure optimization and the electronic structure analysis, we conclude that the published[21] calcium carbide structure for $CaO_2$ is incorrect, at least for pure calcium peroxide (hence the use of parentheses for the structural data of $CaO_2$ in Table III). We addressed this problem in more detail elsewhere[7] by calculating the internal and Gibbs free energies of the peroxide decomposition reaction $MO_2(s) \rightarrow MO(s) + 1/2O_2(g)$ ($M$ = Ba, Sr, Ca), which are clearly negative for $CaO_2$, in contrast to $BaO_2$ and $SrO_2$.

### B. Structures under pressure

We examine now the behavior of the oxides and, in particular, of the peroxides under pressure by considering the bulk moduli and the unit-cell edge and bond compressibilities.

The bulk moduli calculated using the Vinet equation of state (3) are reported in Table III. As observed in Refs. 16 and 17, the errors for CaO and SrO are approximately 8% and 20% in both HF and DFT calculations. However, for BaO we calculated a bulk modulus that is very close to the experimental value. We note that the reported experimental values of the bulk moduli have been extrapolated to 0 K and thus directly correspond to our calculation.

By differentiating the Vinet equation of state (3) with respect to the volume, the pressure as a function of the volume is obtained.

$$p(V) = -\frac{dE}{dV} = 3B_0 e^{\gamma(1-\beta)}\left(\frac{1}{\beta^2} - \frac{1}{\beta}\right). \tag{5}$$

Now, the first- and the second-order compressibility $D_1$ and $D_2$ can be determined for selected structural parameters

$$\frac{r}{r_0}(p) = 1 - D_1 p + D_2 p^2, \tag{6}$$

TABLE IV. Coefficients $D_1$ and $D_2$ of the parabolic approximation $r/r_0 = 1 - D_1 \cdot p + D_2 \cdot p^2$, fitted using the least-squares method for the pressure dependence of the lattice constants and bondlengths (DFT calculations). The coefficient $D_1$ is the first-order compressibility of the bond or cell edge.

| Compound | Barium | | Strontium | | Calcium | |
|---|---|---|---|---|---|---|
| | $D_1(\mathrm{TPa}^{-1})$ | $D_2(\mathrm{TPa}^{-2})$ | $D_1(\mathrm{TPa}^{-1})$ | $D_2(\mathrm{TPa}^{-2})$ | $D_1(\mathrm{TPa}^{-1})$ | $D_2(\mathrm{TPa}^{-2})$ |
| $MO_2$ | | | | | | |
| $a/a_0$ | 3.75 | 66 | 3.43 | 43 | 2.01 | 10 |
| $c/c_0$ | 5.80 | 156 | 3.59 | 35 | 4.29 | 41 |
| $d_{O-O}/d^0_{O-O}$ | 1.78 | 42 | 1.02 | 2 | 1.17 | 7 |
| $D_{M-O}/d^0_{M-O}(2\times)$ | 6.94 | 184 | 4.38 | 43 | 5.32 | 53 |
| $d_{M-O}/d^0_{M-O}(8\times)$ | 3.24 | 44 | 3.28 | 43 | 1.93 | 10 |
| $MO$ | | | | | | |
| $d_{M-O}/d^0_{M-O}$ | 3.41 | 34 | 2.39 | 16 | 2.33 | 15 |

where $r$ may be a unit-cell edge or a bondlength and $r_0$ is the corresponding equilibrium value. The coefficients $D_1$ and $D_2$ obtained using the least squares fitting procedure are reported in Table IV.

We note that the compressibility in the [001] direction of the crystal structure is considerably higher than in the [100] direction as the lattice compressibilities along the $c$ axis and of the $M$—O($2\times$) bond are higher than that along the $a$ axis and of the $M$—O($8\times$) bonds. We also observe that the compressibility of individual bonds decreases when we move from the heavier to the lighter alkaline-earth-metal oxides or peroxides of the same crystal structure. Only $CaO_2$ shows a different behavior clearly related to unusual features in the ionic bonding of this material.

For $BaO_2$ the unit-cell edges and the unit-cell volume, scaled by their equilibrium values, are plotted against pressure in Fig. 6. The lines show the structural parameters fitted using Eqs. (5) and (6). Some of the experimental points[9] are also shown for $p<5$ GPa. Within the range where experimental data are available, the agreement with the theoretical results appears to be excellent for the unit-cell edge $c$, while the compressibilities of the unit-cell edge $a$ and of the volume are slightly underestimated. On the other hand, we note that the experimental data were obtained at room temperature and therefore not directly comparable with the 0 K calculations; the difference indeed could be caused by thermal effects. The trend could also indicate the increased importance of a good description of the interaction between peroxide ions. In particular, the dispersion forces that are not rigorously accounted for in the generalized gradient approximation (GGA)-DFT can contribute to the compressibility.

The DFT results for the compressibility of the peroxide molecular ion (Table IV) reveal that in all peroxide materials investigated, the peroxide bond has the lowest bond compressibility, that is it is calculated to be essentially rigid. The $M$—O($2\times$) bonds, on the contrary, have a bond compressibility that is approximately four times as large as the bond compressibility of the peroxide molecular ion. The neglect of electron correlation in the HF calculations, as we have already seen, leads to a reversed order of the peaks in the DOS of $BaO_2$ corresponding to the $\sigma_z$ molecular orbital and the $\pi_x$ and $\pi_y$ molecular orbitals as compared to the DFT calculations. A further consequence of the HF approximation is that the bond compressibility of the $O_2^{2-}$ ion is considerably smaller compared to the DFT calculations. Thus, we calculated, using the HF method, for $BaO_2$ a bond compressibility of only 0.93 $\mathrm{TPa}^{-1}$ compared with 1.78 $\mathrm{TPa}^{-1}$ from the DFT calculations, and for $SrO_2$ 0.80 $\mathrm{TPa}^{-1}$ compared with the DFT value of 1.02 $\mathrm{TPa}^{-1}$.

## V. CONCLUSIONS

The electronic and structural properties of the alkaline-earth-metal peroxides $BaO_2$, $SrO_2$, and $CaO_2$ are to a great extent determined by the generic properties of the peroxide molecular ion $O_2^{2-}$. The primary aim of this study was to amplify our understanding of the chemical bonding effects within the $O_2^{2-}$ ion and its stabilization by the ionic environment.

The chemical bonding within the peroxide molecular ion has a complex chemical nature, with a balance between the weak covalent bond of $\sigma_z$ type and the strong electrostatic repulsion of the *closed-shell* electron groups occupying O $2s$ and O $2p_x$ and $2p_y$ states. Compression of the peroxide ion in the solid ionic crystals gives rise to an excessive overlap of the O $2s$ closed shells of the two $O^-$ ions of a peroxide

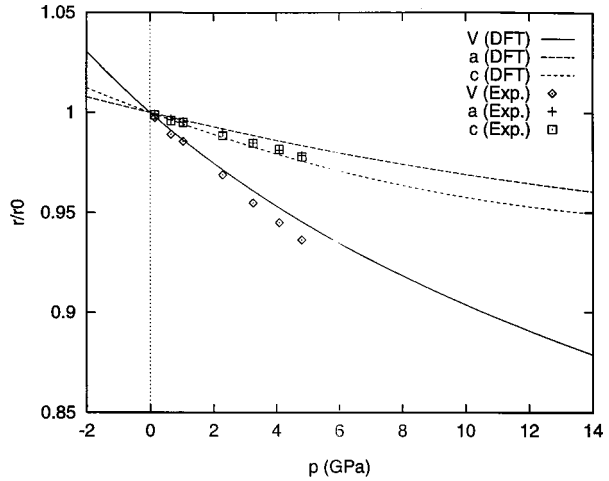


FIG. 6. Unit-cell edges and the unit-cell volume of $BaO_2$, divided by their equilibrium values, as a function of pressure. The DFT notations for the lines represent the DFT energy values fitted using Eq. (6). The Exp. notation stands for the experimental points from Ref. 9.

molecular ion $O_2^{2-}$, which in turn determines *the antibonding character of the interaction and chemical bonding in the* $O_2^{2-}$ *molecular ion*.

The valence charge density on the $O^-$ constituent ions of the peroxy species is significantly polarized by the crystal electrostatic field. An accurate description of the oxygen polarizability seems to be crucial for the reproduction and prediction of the crystal structure and adiabatic surface. The properties affected include the compressibility and energies of vibrational transitions.

The necessity of a good level of theoretical description for the covalent bonding and polarization effects makes the Hartree-Fock approach unsuitable. The GGA-DFT method provides reasonable agreement with the experimental crystal structures; still, the peroxide bond lengths are slightly overestimated by 2.5% in $BaO_2$ and 3.2% in $SrO_2$ respectively. The DFT results, although in agreement with experiment, might depend on the quality of the basis set used. Insufficiently extensive basis sets are known to fail in the description of polarizability, which is an incentive for future work. Furthermore, the analysis of the electronic and structural properties given offers a basis for a derivation of an *ab initio* force field with the aim of a separation of the electrostatic and short-range exchange-correlation interactions in the ionic peroxides.

## ACKNOWLEDGEMENTS

M.K. wishes to thank the DFG (Deutsche Forschungsgemeinschaft) for financial support of this work. N. M. Harrison is gratefully acknowledged for providing the barium valence basis set. We would like to thank F. Corà, A. Shluger, and P. Souchko for many useful discussions and advice.

[1] D. L. Griscom, J. Ceram. Soc. Jpn. **99**, 923 (1991).
[2] V. Priest, D. L. Cowan, H. Ysar, and F. K. Ross, Phys. Rev. B **44**, 9877 (1991).
[3] H. Nakatsui and H. Nakai, Chem. Phys. Lett. **197**, 2423 (1992).
[4] J. M. Savariault and M. S. Lehman, J. Am. Chem. Soc. **102**, 1298 (1980).
[5] G. Moutiers, M. Cassir, and J. Devynck, J. Electroanal. Chem. **324**, 175 (1992).
[6] G. Mestl, M. P. Rosynek, and J. H. Lunsdorf, J. Phys. Chem. B **101**, 9329 (1997).
[7] M. Königstein and C. R. A. Catlow, J. Solid State Chem. **140**, 103 (1998).
[8] F. Föppl, Z. Anorg. Allg. Chem. **291**, 12 (1957).
[9] M. Königstein, Ph.D. thesis, Universität Regensburg, 1996; J. Solid State Chem. **140**, 103 (1998).
[10] N.-G. Vannerberg, Prog. Inorg. Chem. **4**, 125 (1962).
[11] T. Bremm and M. Jansen, Z. Anorg. Allg. Chem. **610**, 64 (1992).
[12] J.-M. Savariault and M. S. Lehmann, J. Am. Chem. Soc. **102**, 1298 (1980).
[13] H. H. Eysel and S. Thym, Z. Anorg. Allg. Chem. **411**, 97 (1975).
[14] A. Lichanot, M. Chaillet, C. Larrieu, R. Dovesi, and C. Pisani, Chem. Phys. **164**, 383 (1992).
[15] R. Dovesi, C. Roetti, C. Freyria-Fava, E. Aprà, V. R. Saunders, and N. M. Harrison, Philos. Trans. R. Soc. London, Ser. A **341**, 203 (1992).
[16] C. Freyria-Fava, F. Dovesi, V. R. Saunders, M. Leslie, and C. Roetti, J. Phys.: Condens. Matter **5**, 4793 (1993).
[17] A. Zupan, I. Petek, M. Causà, and R. Dovesi, Phys. Rev. B **48**, 799 (1993).
[18] P. D. VerNooy, Acta Crystallogr., Sect. C: Cryst. Struct. Commun. **49**, 433 (1993).
[19] W. Wong-Ng and R. S. Roth, Physica C **233**, 97 (1994).
[20] K.-J. Range, F. Rau, U. Schießl, and U. Klement, Z. Anorg. Allg. Chem. **620**, 879 (1994).
[21] V. Kotov and S. I. Reichstein, Zh. Fiz. Khim. **15**, 1057 (1941).
[22] C. Brosset and N.-G. Vannerberg, Nature (London) **177**, 238 (1956).
[23] J. Koput, Chem. Phys. Lett. **236**, 516 (1995).
[24] R. Benassi and F. Taddei, Tetrahedron **50**, 4795 (1994).
[25] R. D. Bach, P. Y. Ayala, and H. B. Schlegel, J. Am. Chem. Soc. **118**, 12 758 (1996).
[26] R. Benassi, L. G. Fiandri, and F. Taddei, J. Org. Chem. **60**, 5855 (1995).
[27] A. H. Edwards and W. B. Fowler, Phys. Rev. B **26**, 6649 (1982).
[28] H. Nakatsuji and H. Nakai, J. Chem. Phys. **98**, 2423 (1993).
[29] H. Donnerberg and A. Birkholz, J. Phys.: Condens. Matter **7**, 327 (1995).
[30] K. N. Fan, W. N. Wang, and J. F. Deng, Bull. Chem. Soc. Jpn. **68**, 3035 (1995).
[31] L. N. Kantorovich and M. Gillan, Mater. Sci. Forum **239**, 637 (1997).
[32] C. Pisani, R. Dovesi, and C. Roetti, *Hartree-Fock ab initio Treatment of Crystalline Systems*, Lecture Notes in Chemistry, Vol. 48 (Springer-Verlag, Heidelberg, 1988).
[33] R. Dovesi, V. R. Saunders, C. Roetti, M. Causà, N. M. Harrison, R. Orlando, and E. Aprà, *CRYSTAL95 User's Manual* (University of Torino, Torino, 1996).
[34] M. Causà and A. Zupan, Int. J. Quantum Chem., Quantum Chem. Symp. **28**, 633 (1994).
[35] J. P. Perdew, in *Electronic Structure of Solids*, edited by P. Ziesche and H. Eschrig (Akademie Verlag, Berlin, 1991).
[36] J. P. Perdew and Y. Wang, Phys. Rev. B **33**, 8800 (1986); **40**, 3399 (1989); **45**, 13 244 (1992).
[37] A. Zupan and M. Causà, Int. J. Quantum Chem. **56**, 337 (1995).
[38] D. R. Haman, Phys. Rev. B **55**, R10 157 (1997).
[39] P. J. Hay and W. R. Wadt, J. Chem. Phys. **82**, 270 (1985); **82**, 284 (1985); **82**, 299 (1985).
[40] N. M. Harrison (private communication).
[41] M. Catti, G. Valerio, R. Dovesi, and M. Causà, Phys. Rev. B **49**, 14 179 (1994).
[42] A. S. Rao and R. J. Kearney, Phys. Status Solidi B **95**, 243 (1979).
[43] M. Springborg and O. E. Taurian, J. Phys. C **19**, 6347 (1986).
[44] R. S. Mulliken, J. Chem. Phys. **36**, 3428 (1962).
[45] R. F. W. Bader, Chem. Rev. **91**, 893 (1991).
[46] K. B. Wiberg and P. R. Rablen, J. Comput. Chem. **14**, 1504 (1993).
[47] R. F. W. Bader and M. A. Austen, J. Chem. Phys. **107**, 4271 (1997).

[48] The results of the calculations of the $H_2O_2$ and $F_2$ molecules, given here for comparison, have been obtained using standard 6-311$G$* basis sets for H and F. The calculations on the oxygen molecule and the peroxide molecular ion have been performed by using essentially the same basis set as for the crystal calculations, which was, however, supplemented by two additional diffuse shells, the exponents of which were optimized. We have performed only a single point calculation on the hydrogen peroxide molecule, the structure of which has been optimized beforehand using a practically converged numerical basis set and the same PW91 density functional.

[49] P. Vinet, J. Ferrante, J. R. Smith, and J. H. Rose, J. Phys. C **19**, L467 (1986).

[50] P. Vinet, J. H. Rose, J. Ferrante, and J. R. Smith, J. Phys.: Condens. Matter **1**, 1941 (1989).

[51] P. E. Sinclair and C. R. A. Catlow, J. Chem. Soc., Faraday Trans. **93**, 333 (1997).

[52] A. Zupan, K. Burke, M. Ernzerhof, and J. P. Perdew, J. Chem. Phys. **106**, 10 184 (1997).

[53] M. D. Towler, N. L. Allan, N. M. Harrison, V. R. Saunders, W. C. Mackrodt, and E. Aprà, Phys. Rev. B **50**, 5041 (1994).

[54] A. R. West, *Solid State Chemistry and its Applications* (Wiley, New York, 1989).

[55] Z. P. Chang and E. K. Graham, J. Phys. Chem. Solids **38**, 1355 (1977).